and may be found at https://doi.org/10.1121/10.0019750

On the low-frequency acoustic center

Samuel D. Bellows[a)] and Timothy W. Leishman

Acoustics Research Group, Department of Physics and Astronomy, Brigham Young University, Provo, Utah 84602, USA

ABSTRACT:

Acousticians typically consider the acoustic center of a source to be the point from which sound waves appear to diverge spherically. Many applications require the center's accurate determination, but its deeper significance and means of assessment have often remained ambiguous. This work revisits the acoustic center and shows how a low-frequency sound radiator with omnidirectional far-field directivity has a center defined by its dipole-to-monopole moment ratio. This definition yields conclusive results for several theoretical sources and highlights the limitations of characterizing the acoustic center only in terms of an equivalent point source.
© 2023 Acoustical Society of America. https://doi.org/10.1121/10.0019750

I. INTRODUCTION

The acoustic source center has been of considerable interest to researchers and practitioners for decades. Standards now describe it as "the position of the virtual point source from which sound pressure varies inversely as distance"[1] and "the point from which … spherical wavefronts … appear to diverge."[2] These concepts apply to transducer calibrations,[3–5] sound attenuation,[6] assessments of anechoic chamber properties,[7,8] source placements for directivity measurements,[9–12] and many other applications in acoustics. The primary focus of the present work is the accurate placement of the low-frequency acoustic center.

Some early treatments of the acoustic center considered a source's far-field directional characteristics.[13–15] However, Trott asserted that a more specific definition is the "locus of the equivalent point source that yields the same far-field pressure in magnitude and phase in a specified direction" rather than "an arbitrary center of rotation for determining the farfield directional response in terms of sound pressure magnitude."[16] Jacobsen *et al.* later noted that most centering definitions seem to be grounded in the "idea of replacing a real, extended source by an equivalent point source."[17] Nevertheless, they argued that the positioning of this equivalent point source is "deceptively simple" since different approaches yield inconsistent results. For example, definitions of the acoustic center based on matching $1/r$ decays,[18–20] phase shifts,[16,21] group delays,[3] or wavefronts[4] produce different acoustic centers for a radially oscillating sphere or a theoretical point source on a sphere—even when the various methods apply to identical sources.[17]

Vanderkooy justified using an equivalent point source by exploiting the location where one takes a multipole expansion of the Kirchhoff–Helmholtz integral equation (KHIE) to remove the dipole moment.[22] If the higher-order (e.g., quadrupole) terms are negligible, only the monopole moment subsequently remains. This concept leads to a global characterization of the sound field rather than an attempted matching of the amplitude decay, phase, or similar properties in specified directions. While Vanderkooy's approach thus provided a unique acoustic center, it required knowledge of the source boundary pressure and particle velocity, which are generally unknown.

Noting that "theoretical results are difficult to work out," Vanderkooy assumed far-field omnidirectional radiation to estimate the acoustic center based on the pressure difference between two equally distant points from the coordinate origin.[22] He did not directly apply the KHIE to determine acoustic centers but showed, via simulations, good agreement with the underlying centering concepts, including constant contours of $1/r$ decay about the center and constant wavefronts. His results also improved near-field agreement with far-field polar patterns whenever a source appropriately aligned with the acoustic center.[23] Near-field measurements of a small loudspeaker verified anticipated quasi-omnidirectional behavior when it rotated about the estimated acoustic center.[22] Thus, contrary to Trott's assertion, Vanderkooy's results suggested that the point of rotation is not arbitrary; its optimal position coincides with the location of the equivalent point source.

Later research improved upon the two-point estimation method and applied the theory to microphones, a point source on a rigid sphere, and measurements of a KEMAR (Knowles Electronic Manikin for Acoustic Research) head-and-torso simulator.[24,25] These efforts showed that the concepts are consequential but applicable only to sources whose radiation patterns become omnidirectional in the far field. They are not particularly beneficial for dipolar, cardioid-like, or more complex patterns.[22]

Aarts and Janssen derived the low-frequency acoustic centers of radially and axially oscillating caps on a rigid sphere using Vanderkooy's two-point estimation method.[26]

a)Electronic mail: samuel.bellows11@gmail.com

Their general formula is a closed-form solution based on Legendre polynomial pressure expansion coefficients, applying to axisymmetric spherical sources with far-field omnidirectional radiation patterns. Their results provided insights into the effects of loudspeaker driver sizes on the acoustic center. However, more general radiation cases remained unresolved.

Because of the importance of acoustic centers for directivity measurements, other authors have attempted to exploit pressure field spherical harmonic expansions to determine their locations.[9–12] Such expansions allow sound field representations of arbitrary sources instead of only axisymmetric spherical sources.[27] However, rather than developing closed-form solutions similar to Aarts and Janssen's solutions, the authors minimized objective functions based on changing spherical harmonic expansion origins to predict the acoustic centers.[9,11] Other efforts incorporated phase differences.[9,12] Because a close relationship exists between the first few multipole terms and spherical harmonic expansions at low frequencies,[27–29] the approaches that minimize higher-order expansion terms[9,11] are somewhat analogous to Vanderkooy's approach of eliminating the dipole moment.

The advantage of these recent techniques is that they deduce an acoustic center directly from data measured by a surrounding spherical microphone array. Thus, the methods apply to measured sources with general radiation patterns. Even so, the approaches come at the cost of computationally expensive optimization procedures that have difficulties centering sources at higher frequencies when the far-field omnidirectional radiation assumption breaks down.[11] In some cases, the phase-based approaches may extend the usable bandwidth.[12]

Despite the importance and applicability of past work in acoustic centering, further conceptual development for general source radiation remains necessary. This work accordingly revisits and expands upon Vanderkooy's discussions and demonstrates that sound radiators with primarily omnidirectional far-field directivity patterns have low-frequency acoustic centers defined by their dipole-to-monopole moment ratios. Additional application of the KHIE to the sphere reveals that these moments follow from the spherical harmonic expansion coefficients of the surface particle velocities. A proposed centering method yields closed-form solutions for the low-frequency acoustic centers of several theoretical sources. It also produces center-of-mass–like formulas and provides bounds on acoustic center locations relative to source geometries. The results are general enough to handle axisymmetric and nonaxisymmetric radiation.

After exploring the theoretical concept of the low-frequency acoustic center and providing several clarifying examples, the following sections generalize low-frequency acoustic centering to arbitrarily shaped sources via spherical harmonic expansion coefficients of radiated pressure fields and multipole moments. The generalization yields the acoustic center through a closed-form solution rather than an optimization procedure. The approach is thus applicable to measurements made by surrounding spherical microphone arrays, which are becoming increasingly ubiquitous for measuring sound radiation from arbitrarily-shaped sources. Experimental results based on a KEMAR head and torso simulator (HATS) validate the proposed technique and show it to be in excellent agreement with the optimization procedures developed in previous works. The results enhance theoretical understanding and will improve the practical applications of acoustic centering.

II. THEORY OF THE LOW-FREQUENCY ACOUSTIC CENTER

Consider an arbitrary acoustic source radiating into free space as suggested by Fig. 1. The KHIE with no volume sources present yields the complex pressure amplitude on the exterior domain as a function of the normal particle velocity $u_n(\mathbf{r}_s)$ and surface pressure $p(\mathbf{r}_s)$ on the boundary S:[30]

$$p(\mathbf{r}) = \int\int_S \left[iz_0 k u_n(\mathbf{r}_s) G(\mathbf{r}, \mathbf{r}_s) + \frac{\partial}{\partial n_s} G(\mathbf{r}, \mathbf{r}_s) p(\mathbf{r}_s) \right] dS, \quad (1)$$

where

$$G(\mathbf{r}, \mathbf{r}_s) = \frac{e^{-ik|\mathbf{r}-\mathbf{r}_s|}}{4\pi|\mathbf{r}-\mathbf{r}_s|} \quad (2)$$

is the free space Green's function, $z_0 = \rho_0 c$ is the characteristic specific acoustic impedance of the medium, and k is the wavenumber. This convention assumes the normal direction is into the domain and assumes $e^{i\omega t}$ time dependence.

If the source falls within a notional observation sphere of radius a, indicated by the dashed circle in Fig. 1, a Taylor's series expansion of the free-space Green's function about the point $\mathbf{r}''$ sets up a convergent series of multipole moments when $ka \ll 1$.[30] Considering only the first two terms of the expansion, the monopole and dipole terms, the pressure becomes

$$p(\mathbf{r}) \approx MG(\mathbf{r}, \mathbf{r}'') + ikG(\mathbf{r}, \mathbf{r}'')\left(1 - \frac{i}{kR}\right) \mathbf{D}(\mathbf{r}'') \cdot \hat{\mathbf{R}}, \quad (3)$$
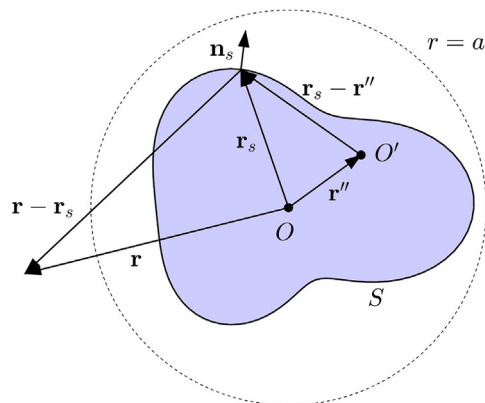

FIG. 1. (Color online) Diagram of a radiating source with position and translation vectors.

J. Acoust. Soc. Am. **153** (6), June 2023

Samuel D. Bellows and Timothy W. Leishman   3405

where M is the monopole moment

$$M = iz_0k \iint_S u_n(\mathbf{r}_s)dS, \qquad (4)$$

$\mathbf{D}$ is the dipole moment

$$\mathbf{D}(\mathbf{r}'') = \iint_S \left[iz_0k(\mathbf{r}_s - \mathbf{r}'')u_n(\mathbf{r}_s) + \hat{\mathbf{n}}_s p(\mathbf{r}_s)\right]dS, \qquad (5)$$

$\mathbf{R} = \mathbf{r} - \mathbf{r}''$, and $\hat{\mathbf{R}}$ is the unit vector in the direction of $\mathbf{R}$. While the monopole moment is invariant to the point about which one takes the Taylor's series expansion, the dipole and higher-order moments are not.

To replace an extended source by a single point source, Vanderkooy allowed the expansion origin to vary.[22] He defined the acoustic center $\mathbf{r}_c$ as the expansion origin ($\mathcal{O}'$ in Fig. 1) about which the dipole moment vanishes, i.e.,

$$\mathbf{D}(\mathbf{r}_c) = \mathbf{0}. \qquad (6)$$

When $\mathbf{r}'' = \mathbf{r}_c$, Eq. (3) then reduces to the simple form

$$p(\mathbf{r}) \approx MG(\mathbf{r}, \mathbf{r}_c). \qquad (7)$$

This equation describes the field of a point source located at the acoustic center $\mathbf{r}_c$ whose strength is proportional to the volume velocity of the original source; it is analogous to Eq. (1) of Jacobsen et al.[17] Thus, at low frequencies, it is possible to replace a "real, extended source by an equivalent point source,"[17] simply by exploiting the point of KHIE multipole expansion.

With some deviations to Vandkerooy's solution for $\mathbf{r}_c$, one may express the acoustic center in terms of the monopole and dipole moments. First, note that Eq. (5) may be expressed as

$$\mathbf{D}(\mathbf{r}'') = \iint_S [iz_0k\mathbf{r}_s u_n(\mathbf{r}_s) + \hat{\mathbf{n}}_s p(\mathbf{r}_s)]dS$$
$$- \mathbf{r}''iz_0k\iint_S u_n(\mathbf{r}_s) = \mathbf{D}(\mathbf{0}) - \mathbf{r}''M, \qquad (8)$$

where

$$\mathbf{D}(\mathbf{0}) = \iint_S [iz_0k\mathbf{r}_s u_n(\mathbf{r}_s) + \hat{\mathbf{n}}_s p(\mathbf{r}_s)]dS \qquad (9)$$

is the dipole moment with the origin as the expansion point. This equation describes the relationship between the dipole moment expanded at the origin and the dipole moment expanded at $\mathbf{r}''$. Moving the expansion origin to $\mathbf{r}''$ decreases the dipole moment by $\mathbf{r}''M$. Consequently, a poor expansion origin choice can artificially inflate the magnitude of the dipole moment. In contrast, choosing the expansion origin as the acoustic center minimizes higher-order contributions and yields the simplest representation of the pressure field. Substituting Eq. (6) into Eq. (8) and solving for the acoustic center yields

$$\mathbf{r}_c = \frac{\mathbf{D}(\mathbf{0})}{M}. \qquad (10)$$

Thus, one may define the low-frequency acoustic center simply as the dipole-to-monopole moment ratio.

This formula is effective for sources whose far-field radiation patterns are approximately omnidirectional, i.e., such that Eq. (7) yields an adequate representation of the far-field pressure. However, it does not restrict near-field directional patterns. Because the derivation requires $\mathbf{D}(\mathbf{r}_c) = \mathbf{0}$, it cannot apply to sources that produce dipole, cardioid, or more complex far-field patterns. Nevertheless, far-field omnidirectional radiation is common to many sources at low frequencies, including loudspeakers,[31–33] speech,[34–36] and some musical instruments.[37–40] Reciprocity extends the approach to sound receivers with low-frequency omnidirectional reception, including certain microphones[31,41,42] and the human head.[25,43–45]

While one typically considers an acoustic center to be a real-valued quantity, Eq. (10) allows the possibility of a complex value in some cases. The following sections touch on this characteristic, which previous studies overlooked, but a complete understanding of its significance and ramifications requires additional research beyond the scope of the present work.

III. APPLICATION TO SPHERICAL SOURCE CONFIGURATIONS

Although Eq. (10) provides a straightforward method to determine the acoustic center, calculating $\mathbf{D}(\mathbf{0})$ and M requires surface integrals involving the normal particle velocity and pressure, which are often unknown. This difficulty led Vanderkooy to adopt his fitting procedure for measured pressure values rather than evaluating the integrals. In their work on spheres with oscillating caps, Aarts and Janssen did not directly evaluate the surface integrals either. However, this section shows that sources with spherical geometries have spherical harmonic expansion coefficients for their normal surface velocity and matched particle velocity distributions that relate closely to the monopole and dipole moments. They consequently allow low-frequency acoustic centering via closed-form solutions.

If the surface S is that of a sphere of radius a, Eq. (4) becomes

$$M = iz_0ka^2 \int_0^{2\pi} \int_0^{\pi} u_n(\theta, \phi) \sin\theta d\theta d\phi \qquad (11)$$

and Eq. (9) becomes

$$\mathbf{D}(\mathbf{0}) = a^2 \int_0^{2\pi} \int_0^{\pi} \hat{\mathbf{r}}_s[iz_0ka u_n(\theta, \phi) + p(\theta, \phi)]\sin\theta d\theta d\phi, \qquad (12)$$

where $\hat{\mathbf{r}}_s = \mathbf{r}_s/a$ is the outward-pointing unit normal vector. Spherical harmonic expansions applied to the normal particle velocity and pressure further simplify these integrals.

The normalized spherical harmonics

$$Y_n^m(\theta,\phi) = \sqrt{\frac{2n+1}{4\pi}\frac{(n-m)!}{(n+m)!}}P_n^m(\cos\theta)e^{im\phi} \tag{13}$$

of degree n and order m constitute an orthogonal basis on the sphere.[46] Here, P_n^m are the associated Legendre functions, which include the Condon–Shortley phase. Because the following derivation and subsequent applications employ spherical harmonics of degrees $n=0$ and $n=1$ extensively, Table I includes their definitions for convenience.

The normal particle velocity at the spherical surface has the expansion

$$u_n(\theta,\phi) = \sum_{n=0}^{\infty}\sum_{m=-n}^{n} U_n^m Y_n^m(\theta,\phi), \tag{14}$$

where

$$U_n^m = \int_0^{2\pi}\int_0^{\pi} u_n(\theta,\phi)\left[Y_n^m(\theta,\phi)\right]^* \sin\theta d\theta d\phi \tag{15}$$

and * denotes complex conjugation. To find the monopole moment, one may substitute Eq. (14) into Eq. (11) to produce the result

$$M = iz_0 ka^2 \sum_{n=0}^{\infty}\sum_{m=-n}^{n} U_n^m \int_0^{2\pi}\int_0^{\pi} Y_n^m(\theta,\phi)\sin\theta d\theta d\phi. \tag{16}$$

With the integrand factor $1 = \sqrt{4\pi}[Y_0^0(\theta,\phi)]^*$ (see Table I), orthogonality conditions yield

$$\int_0^{2\pi}\int_0^{\pi} Y_n^m(\theta,\phi)\sin\theta d\theta d\phi = \sqrt{4\pi}\,\delta_{n,0}^{m,0}, \tag{17}$$

where $\delta_{n,n'}^{m,m'}$ is the Kronecker delta, such that

$$M = iz_0 ka^2 \sqrt{4\pi}\,U_0^0. \tag{18}$$

The dipole moment requires the surface pressure distribution in addition to the velocity distribution. Applying Euler's equation to the exterior solution of the Helmholtz equation (Ref. 27) yields

$$p(\theta,\phi) = -iz_0 \sum_{n=0}^{\infty}\sum_{m=-n}^{n} U_n^m \frac{h_n^{(2)}(ka)}{h_n^{(2)\prime}(ka)} Y_n^m(\theta,\phi), \tag{19}$$

TABLE I. Definitions of four normalized spherical harmonics commonly used in this work.

$Y_0^0(\theta,\phi)$	$\sqrt{\dfrac{1}{4\pi}}$
$Y_1^{-1}(\theta,\phi)$	$\sqrt{\dfrac{3}{8\pi}}\sin\theta e^{-i\phi}$
$Y_1^0(\theta,\phi)$	$\sqrt{\dfrac{3}{4\pi}}\cos\theta$
$Y_1^1(\theta,\phi)$	$-\sqrt{\dfrac{3}{8\pi}}\sin\theta e^{i\phi}$

where $h_n^{(2)}(ka)$ are the spherical Hankel functions of the second kind. Substituting Eqs. (19) and (14) into Eq. (12) then produces the dipole moment

$$\mathbf{D}(\mathbf{0}) = iz_0 a^2 \sum_{n=0}^{\infty}\sum_{m=-n}^{n} U_n^m\left[ka - \frac{h_n^{(2)}(ka)}{h_n^{(2)\prime}(ka)}\right]$$
$$\times \int_0^{2\pi}\int_0^{\pi}\hat{\mathbf{r}}_s Y_n^m(\theta,\phi)\sin\theta d\theta d\phi. \tag{20}$$

From Table I,

$$\hat{\mathbf{r}}_s = \begin{bmatrix} x_s/a \\ y_s/a \\ z_s/a \end{bmatrix} = \begin{bmatrix} \sin\theta\cos\phi \\ \sin\theta\sin\phi \\ \cos\theta \end{bmatrix}$$
$$= \sqrt{\frac{2\pi}{3}}\begin{bmatrix} Y_1^{-1}(\theta,\phi) - Y_1^1(\theta,\phi) \\ i(Y_1^{-1}(\theta,\phi) + Y_1^1(\theta,\phi)) \\ \sqrt{2}Y_1^0(\theta,\phi) \end{bmatrix}^*. \tag{21}$$

Consequently, the orthogonalities of the respective spherical harmonics simplify the integral to

$$\int_0^{2\pi}\int_0^{\pi}\hat{\mathbf{r}}_s Y_n^m(\theta,\phi)\sin\theta d\theta d\phi = \sqrt{\frac{2\pi}{3}}\begin{bmatrix} \delta_{n,1}^{m,-1} - \delta_{n,1}^{m,1} \\ -i(\delta_{n,1}^{m,-1} + \delta_{n,1}^{m,1}) \\ \sqrt{2}\delta_{n,1}^{m,0} \end{bmatrix}. \tag{22}$$

Substituting this result into Eq. (20) then gives the result

$$\mathbf{D}(\mathbf{0}) = iz_0 a^2 \sqrt{\frac{2\pi}{3}}\left[ka - \frac{h_1^{(2)}(ka)}{h_1^{(2)\prime}(ka)}\right]\begin{bmatrix} U_1^{-1} - U_1^1 \\ -i(U_1^{-1} + U_1^1) \\ \sqrt{2}U_1^0 \end{bmatrix}. \tag{23}$$

While Eq. (23) is valid for all frequencies, the small-argument approximations[46]

$$h_n^{(2)}(ka) \approx i\frac{(2n)!}{2^n n!}\frac{1}{(ka)^{n+1}}, \quad ka \ll 1 \tag{24}$$

and

$$h_n^{(2)\prime}(ka) \approx -i(n+1)\frac{(2n)!}{2^n n!}\frac{1}{(ka)^{n+2}}, \quad ka \ll 1 \tag{25}$$

provide further simplification at low frequencies. The ratio of the spherical Hankel function and its derivative simplifies to

$$\frac{h_n^{(2)}(ka)}{h_n^{(2)\prime}(ka)} \approx -\frac{ka}{(n+1)}, \quad ka \ll 1, \tag{26}$$

such that the dipole moment becomes

J. Acoust. Soc. Am. **153** (6), June 2023

Samuel D. Bellows and Timothy W. Leishman   3407

$$\mathbf{D}(\mathbf{0}) = iz_0 \frac{3}{2} ka^3 \sqrt{\frac{2\pi}{3}} \begin{bmatrix} U_1^{-1} - U_1^1 \\ -i(U_1^{-1} + U_1^1) \\ \sqrt{2}U_1^0 \end{bmatrix}. \tag{27}$$

Finally, the substitution of Eqs. (18) and (27) into Eq. (10) yields the acoustic center

$$\mathbf{r}_c = \frac{a}{2U_0^0} \sqrt{\frac{3}{2}} \begin{bmatrix} U_1^{-1} - U_1^1 \\ -i(U_1^{-1} + U_1^1) \\ \sqrt{2}U_1^0 \end{bmatrix}. \tag{28}$$

This result is significant because it presents a closed-form solution for the low-frequency acoustic center of a generally vibrating spherical source, and it is straightforwardly dependent on only a few particle velocity expansion coefficients.

For axisymmetric spherical sources, $U_n^m = 0$ when $m \neq 0$, so it is common to express the normal surface velocities in terms of Legendre polynomials for the $m = 0$ terms:

$$u_n(\theta) = \sum_{n=0}^{\infty} V_n P_n(\cos\theta). \tag{29}$$

The expansion coefficients V_n relate to the spherical harmonics expansion coefficients via the addition[46]

$$U_n^m = V_n \frac{4\pi}{(2n+1)} \left[Y_n^m(\theta_0, \phi_0)\right]^*, \tag{30}$$

where (θ_0, ϕ_0) is the configuration rotation angle. With no rotation, the source remains axisymmetric about $\hat{\mathbf{z}}$, such that $(\theta_0, \phi_0) = (0, 0)$, $U_0^0 = \sqrt{4\pi}\,V_0$, and $U_1^0 = \sqrt{4\pi/3}\,V_1$ (see Table I). The expression for the acoustic center then simplifies to

$$\mathbf{r}_c = a\frac{V_1}{2V_0}\hat{\mathbf{z}}, \tag{31}$$

which concurs with Eq. (40) of Ref. 26.

IV. EXAMPLES OF SPHERICAL SOURCE CONFIGURATIONS

A radially oscillating sphere,[30] a point source on a sphere,[28] a radially vibrating cap on a sphere,[28,31] and an axially vibrating cap on a sphere[31,47] all represent sources with known expansion coefficients. This section explores the low-frequency acoustic centers of these sources and those of other interesting configurations involving more than one point source on a rigid sphere.

A. Radially oscillating sphere

A radially oscillating sphere of radius a is a prototypical omnidirectional radiator with simple symmetry and uniform normal surface velocity $u_n(\theta, \phi) = u_0$. Its velocity expansion coefficients are all zero except $U_0^0 = u_0\sqrt{4\pi}$. Equation (28) thus requires that $\mathbf{r}_c = \mathbf{0}$, meaning the low-frequency acoustic center falls at the sphere's center, as

suggested by its symmetry. When $ka \ll 1$, the sphere behaves as a simple source at the geometric origin.[30]

B. One point source on a rigid sphere

The radiation from a point source on a rigid sphere is an important case because it yields the Green's function for the associated geometry.[27] It also illustrates basic diffraction effects[48] and has applications in areas such as the simple modeling of head-related transfer functions.[24,25,49]

The velocity expansion coefficients for a point source of strength Q_s and position (θ_s, ϕ_s) on the sphere are[27]

$$U_n^m = \frac{Q_s}{a^2} \left[Y_n^m(\theta_s, \phi_s)\right]^*. \tag{32}$$

The monopole moment [Eq. (18)] is then

$$M = iz_0 k Q_s \tag{33}$$

and the dipole moment [see Eqs. (21) and (27)] is

$$\mathbf{D}(\mathbf{0}) = iz_0 \frac{3}{2} ka Q_s \hat{\mathbf{r}}_s, \tag{34}$$

where $\hat{\mathbf{r}}_s$ is the unit vector in the direction of (θ_s, ϕ_s) (compare Ref. 27, p. 216). The acoustic center follows from Eq. (10) as

$$\mathbf{r}_c = \frac{3}{2} a \hat{\mathbf{r}}_s. \tag{35}$$

Vanderkooy used a numerical example of his method to estimate the low-frequency acoustic center of a point source on the surface of a 170 mm diameter rigid sphere. The calculated center fell at 42.4 mm,[25] which has an implicit value of $r_c = 1.50a$, consistent with Eq. (35).

Figure 2 shows the concurrence of this center with results presented by Jacobsen et al.[17] Their work evaluated three methods for determining the acoustic center of a point source on a rigid sphere. The solid black curve represents the acoustic center based on matching the amplitude of an equivalent point source [Eq. (18) of Ref. 17], the dashed red curve represents the acoustic center based on a reciprocal $1/r$ decay fit [Eq. (19) of Ref. 17], and the dot-dash blue curve represents the acoustic center based on a phase approach [Eq. (21) of Ref. 17]. In all cases, the far-field observation distance is $r = 1$ km.

In the low-frequency limit, amplitude matching approaches converge to the center given by Eq. (35), represented by the dotted green line. Additionally, both methods converge to the same value at all frequencies for the far-field observation distance. As discussed in Jacobsen et al.,[17] the phase method places the acoustic center behind the source. However, modifying the phase method by multiplying the numerator and denominator in Jacobsen et al.[17] [Eq. (21)] by a factor of −1 restricted the inverse tangent to only positive phase values. The resultant acoustic center appears as the purple curve with diamond markers; it does converge to the low-frequency limit. Additionally, this modified result
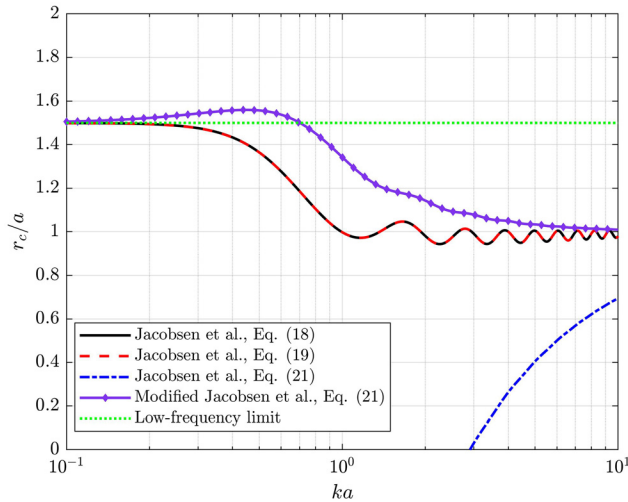
Samuel D. Bellows and Timothy W. Leishman

FIG. 2. (Color online) The acoustic center of a point source on a sphere over dimensionless ka, where a is the sphere's radius.

FIG. 3. (Color online) Sound pressure field for $ka = 0.01$ around (a) a point source on a rigid sphere and (b) its equivalent point source.

more closely follows the trends of the other two methods compared to the unmodified version. Because the formulations of the present work apply only to low-frequency radiation, deviations in the acoustic center's position occur for larger ka. However, the phase-based method does not concur with the two amplitude-matching methods in this range, highlighting the ambiguity in replacing a distributed source with an equivalent point source at higher frequencies.[17]

Figure 3(a) depicts the pressure field surrounding a point source on a rigid sphere for $ka = 0.01$. The figure includes contours in 3 dB increments to illustrate the constant $1/r$ decay. The green dot represents the acoustic center, and the green dashed circle represents a sphere of radius $5a$. The latter aligns well with the contours of constant $1/r$ decay, which is a necessary validation of the acoustic center's location. For this example, the near-field pattern is directional, and the acoustic center lies away from the sphere. However, with sufficient distance, the directivity converges to an omnidirectional far-field pattern. Figure 3(b) depicts the pressure field produced by an equivalent point source in free space. The far-field agreement between both fields highlights the method's effectiveness for low frequencies.

C. Radially oscillating cap on a rigid sphere

The radially oscillating cap on a rigid sphere[28] has helped researchers better understand the radiation of speech, loudspeakers, horns, and other sources.[31,32,36,50,51] It also bridges the two examples in Secs. IV A and IV B. In the limiting case that the cap angle approaches 0 (θ_c to 0), the arrangement behaves as a point source on the sphere. However, when $\theta_c \to \pi$, it behaves as a radially oscillating sphere.

For a cap oriented toward the zenith, $u_n(\theta, \phi) = u_0$ for $0 < \theta < \theta_c$ and zero otherwise. The first two Legendre polynomial series expansion coefficients are then[28,31] $V_0 = u_0(1 - \cos \theta_c)/2$ and $V_1 = 3u_0(1 - \cos^2 \theta_c)/4$, which yield the acoustic center $\mathbf{r}_c(\theta_c) = 3a(1 + \cos \theta_c)\hat{\mathbf{z}}/4$ via Eq.
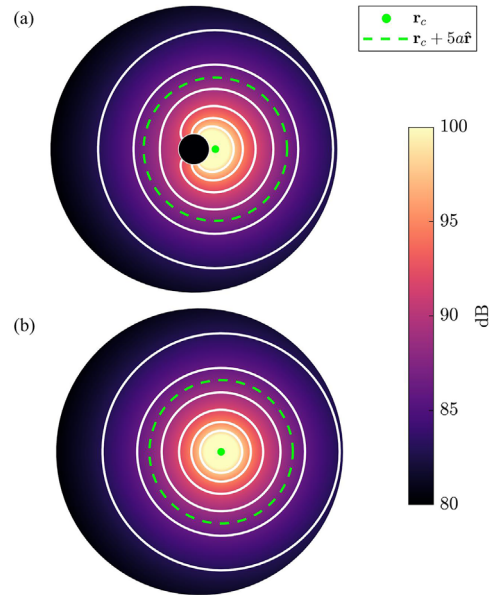
(31), in agreement with the result of Aarts and Janssen.[26] This function appropriately interpolates the acoustic center between $r_c = 3a/2$ and $r_c = 0$, the limiting $\theta_c \to 0$ and $\theta_c \to \pi$ cases, respectively.

Figure 4(a) depicts the acoustic pressure field around the source configuration for $ka = 0.01$ and $\theta_c = \arccos(1/3)$, so that the acoustic center lies at $r_c = a$. Figure 4(b) shows the pressure field produced by an equivalent point source in free space. Although there is significant diffraction around the sphere, the pressure produced by the equivalent point source at the acoustic center shows good far-field agreement.

D. Axially oscillating cap on a rigid sphere

An axially oscillating cap on a rigid sphere is another instructive example. A very small cap angle again produces the pressure field of a point source on a sphere, but a large cap angle $\theta_c \to \pi$ forms a transversely oscillating sphere with a significant dipole moment.[30] Attempting to replace a dipole field with a monopole field is equivocal, so one may anticipate that Eq. (28) diverges as $\theta_c \to \pi$ and $M \to 0$. This condition highlights a potential weakness of defining the acoustic center only in terms of the locus of an equivalent point source.

The normal surface velocity of an axially vibrating cap is $u_n(\theta, \phi) = u_0 \cos \theta$ for $0 < \theta < \theta_c$ and zero otherwise. The first two Legendre polynomial series expansion coefficients are[31,47] $V_0 = u_0(1 - \cos^2 \theta_c)/4$ and $V_1 = u_0(1 - \cos^3 \theta_c)/2$, which give the acoustic center $\mathbf{r}_c(\theta_c) = a(1 + \cos \theta_c + \cos \theta_c^2)\hat{\mathbf{z}}/(1 + \cos \theta_c)$ via Eq. (35), in agreement with the result of Aarts and Janssen.[26]

Figure 5 plots the acoustic center as a function of the cap angle from the zenith for the radially and axially vibrating caps. The acoustic center of the radially vibrating cap, shown as the blue dashed line, interpolates between the two limiting
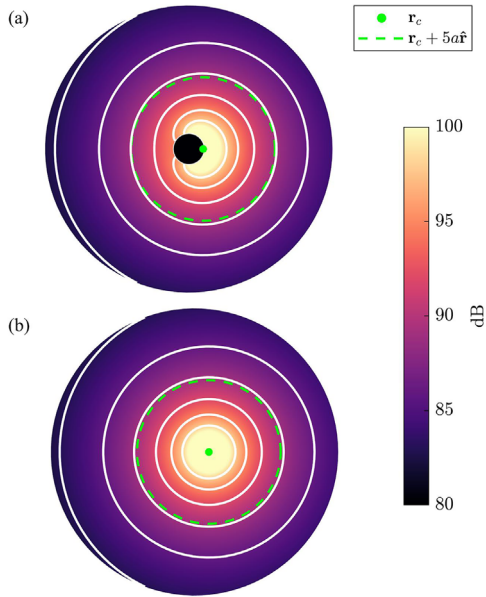
FIG. 4. (Color online) Sound pressure field for $ka = 0.01$ around (a) a radially oscillating cap with cap angle $\theta_c = \arccos(1/3)$ on a rigid sphere and (b) its equivalent point source.

FIG. 6. (Color online) Sound pressure field for $ka = 0.01$ around (a) an axially oscillating cap with cap angle $\theta_c = 0.7\pi$ on a rigid sphere and (b) its equivalent point source.

values, shown as horizontal black dashed lines, of $r_c = 3a/2$ and $r_c = 0$. As for the radially vibrating cap, when $\theta_c \to 0$, the acoustic center of the axially vibrating cap, shown as a solid green line, becomes that of a point source on the sphere. However, as $\theta_c \to \pi$, $M \to 0$ [see Eqs. (4) and (11)], and $r_c \to \infty$ [see Eq. (10)]. The vertical dotted red line marks the threshold up to which $u_n(\theta, \phi) \geq 0$; in the range $\pi/2 < \theta \leq \theta_c$, $u_n(\theta, \phi)$ takes on a 180° phase shift. Consequently, as θ_c increases beyond $\pi/2$, the monopole moment progressively diminishes and the acoustic center moves significantly farther from the sphere's geometric center.

Figure 6(a) depicts the pressure field around the sphere for $ka = 0.01$ and $\theta_c = 0.7\pi = 126°$. The plot shows
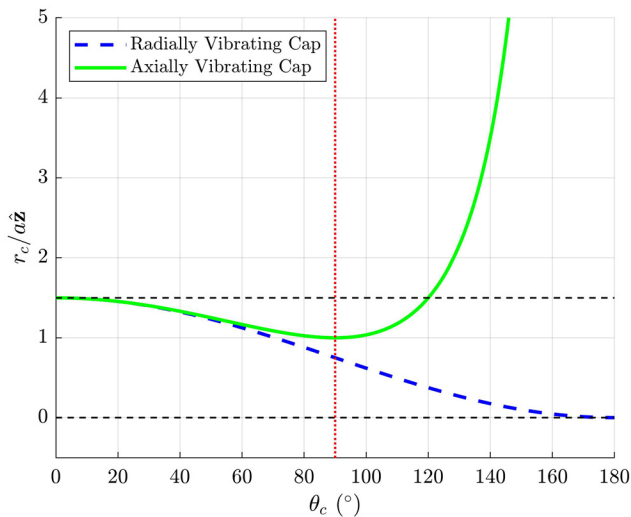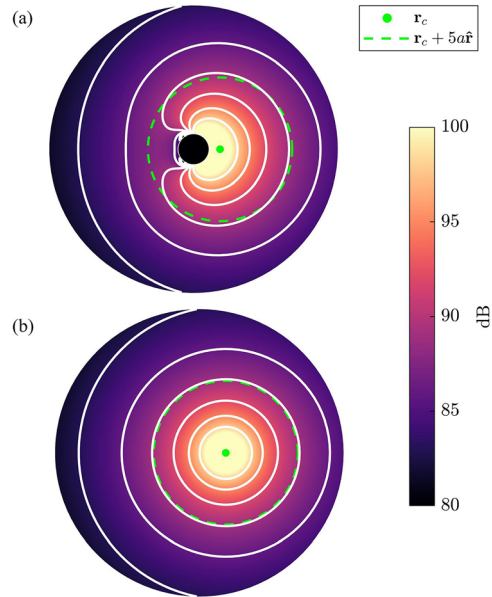
considerable near-field interference, diffraction, and the acoustic center at $r_c = 1.84a$. Figure 6(b) shows the pressure field produced by an equivalent point source in free space. Despite the very directional near-field pattern in Fig. 6(a), as the observation distance increases to the far field, the radiated fields agree and are omnidirectional.

E. Two point sources on a rigid sphere

The concept of substituting a point source for a real source is only valid in the far field when the directivity pattern is omnidirectional. The radiation from two point sources at opposing poles of a rigid sphere helps clarify the difficulty introduced by a dipole moment. As in Sec. IV B, the first source at $(\theta_s, \phi_s) = (0, 0)$ has strength Q_s. The second source at $(\theta_s, \phi_s) = (\pi, 0)$ has strength γQ_s, where γ may vary as a real number. Through superposition, the velocity expansion coefficients become

$$U_n^m = \frac{Q_s}{a^2} \left([Y_n^m(0,0)]^* + \gamma [Y_n^m(\pi,0)]^* \right). \tag{36}$$

However, because the source is axisymmetric, all $m \neq 0$ terms vanish. Equation (13) and the relation $P_n^0(-1) = (-1)^n$ then lead to the result

$$U_n^0 = \frac{Q_s}{a^2} \sqrt{\frac{2n+1}{4\pi}} [1 + \gamma(-1)^n], \tag{37}$$

such that

$$U_0^0 = \frac{Q_s}{a^2} \sqrt{\frac{1}{4\pi}} (1 + \gamma) \tag{38}$$

FIG. 5. (Color online) Low-frequency acoustic centers of a radially and axially oscillating cap on a sphere as a function of cap angle θ_c.

Samuel D. Bellows and Timothy W. Leishman

and

$$U_1^0 = \frac{Q_s}{a^2}\sqrt{\frac{3}{4\pi}}(1-\gamma). \tag{39}$$

The acoustic center follows from Eqs. (30) and (31) as

$$\mathbf{r}_c = \frac{3}{2}a\left(\frac{1-\gamma}{1+\gamma}\right)\hat{\mathbf{z}}. \tag{40}$$

This expression also follows from Eqs. (33) and (34), since by superposition, the net monopole moment is $M = iz_0kQ_s(1+\gamma)$ and the net dipole moment is $\mathbf{D} = iz_0kQ_s3/2a(1-\gamma)\hat{\mathbf{z}}$.

Figure 7 plots the acoustic center as a function of the source strength ratio γ and shows several significant trends. First, when the second source's strength is much larger than the first ($|\gamma| \gg 1$), the acoustic center converges to a single point at $(\theta_0, \phi_0) = (\pi, 0)$, such that $\mathbf{r}_c = -3a/2\hat{\mathbf{z}}$. Second, when the second source's strength is zero ($\gamma = 0$), the acoustic center is that of a single point source located at $(\theta_0, \phi_0) = (0, 0)$, such that $\mathbf{r}_c = 3a/2\hat{\mathbf{z}}$. Third, the acoustic center falls at the center of the sphere when the second source's strength equals the first ($\gamma = 1$), as one might anticipate from symmetry. Fourth, when the two amplitudes are equal but the polarities are opposite ($\gamma = -1$), the acoustic center has an infinite discontinuity to $-\infty$ as $\gamma \to -1^-$ and $+\infty$ as $\gamma \to -1^+$.

The potentially large acoustic center radii for $\gamma \to 1$ in Fig. 7 do not necessarily suggest a nonphysical situation, provided that the source remains nearly omnidirectional in the far field. Figure 8 depicts the pressure field produced by the two point sources for $ka = 0.01$ and $\gamma = -0.8$. The plot ranges over $240a$ in both the x- and y-directions. As in Fig. 3, the contours of equal $1/r$ decay appear in 3 dB increments; however, near the source configuration, which appears as a small black dot, the contours are missing for better visualization.

The cardioid-like equal-level contours in the near field suggest a strong dipole component, which moves the acoustic center to $r_c = 13.5a$, a significant distance from the sphere. Nevertheless, as suggested by the circular contours in the far field, this position coincides with the origin of spherical wavefronts of constant amplitude. The pattern evolution from the near field to the far field apparently requires about $50a$ of propagation. In fact, because $ka = 0.01$, the acoustic far field lies beyond $100a$.

F. Multiple point sources on a rigid sphere and related extensions

Equations (33) and (34) further generalize the result in Eq. (40) to N point sources at arbitrary locations on a sphere. From

$$M = iz_0ka^2\left(\sum_{i=1}^{N}Q_i\right) \tag{41}$$

and

$$\mathbf{D}(0) = iz_0ka^2\left(\frac{3}{2}a\sum_{i=1}^{N}Q_i\hat{\mathbf{r}}_i\right), \tag{42}$$

the acoustic center becomes

$$\mathbf{r}_c = \frac{3}{2}a\left(\frac{\sum_{i=1}^{N}Q_i\hat{\mathbf{r}}_i}{\sum_{i=1}^{N}Q_i}\right). \tag{43}$$

If the relative source strength ratios of all point sources are real valued, i.e., either in phase or 180° out of phase, the acoustic center likewise remains real valued as in Sec. IV E. Other source strength configurations could lead to a
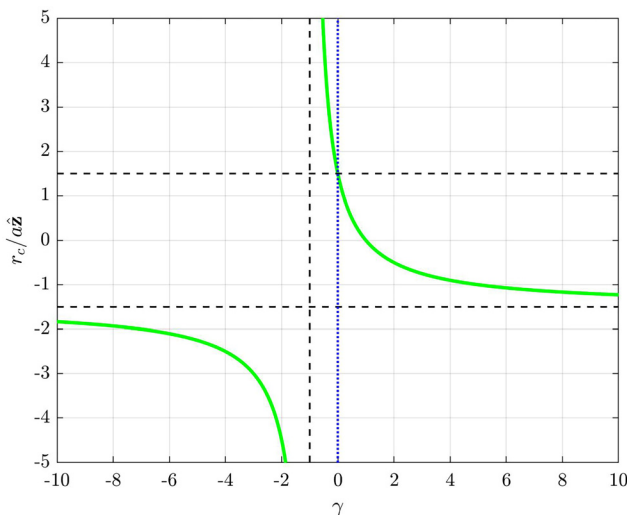

FIG. 7. (Color online) Low-frequency acoustic center predicted by Eq. (28) for two point sources at the opposing poles of a sphere as a function of the second source's relative strength.
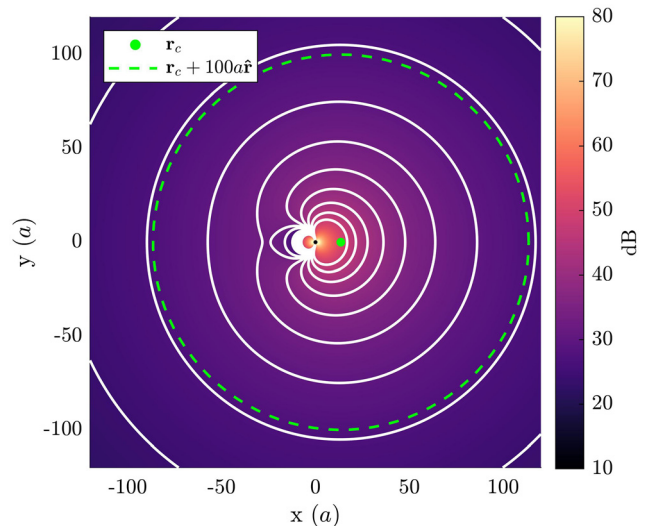

FIG. 8. (Color online) Sound pressure field for $ka = 0.01$ produced by two point sources at the opposing poles of a rigid sphere with a source strength ratio of $\gamma = -0.8$.

J. Acoust. Soc. Am. **153** (6), June 2023

Samuel D. Bellows and Timothy W. Leishman   3411

complex-valued acoustic center (see Sec. VII). A striking feature of this equation is that it simplifies the challenge of determining $\mathbf{D}(\mathbf{0})$ from required surface pressure and velocity distributions. Spherical harmonics and spherical Hankel functions recast the dipole moment only in terms of source strengths and associated local surface velocities.

To better understand why a knowledge of the surface pressure p_i for the ith source is unnecessary, one may work backwards from Eq. (42) to show that

$$\mathbf{D}(\mathbf{0}) = a^3 \sum_{i=1}^{N} \left(i z_0 k \frac{3}{2} Q_i \hat{\mathbf{r}}_i \right) \tag{44}$$

$$= a^3 \sum_{i=1}^{N} \left(i z_0 k Q_i \hat{\mathbf{r}}_i + \frac{1}{2} i z_0 k Q_i \hat{\mathbf{r}}_i \right). \tag{45}$$

For the ith point source, the sifting property yields

$$\int_0^{2\pi} \int_0^{\pi} Q_i \hat{\mathbf{r}}_s \delta(\cos\theta - \cos\theta_i)\delta(\phi - \phi_i)\sin\theta d\theta d\phi = Q_i \hat{\mathbf{r}}_i, \tag{46}$$

so it is also true, by definition [see Eq. (12)], that

$$\mathbf{D}(\mathbf{0}) = a^3 \sum_{i=1}^{N} \left[i z_0 k Q_i \hat{\mathbf{r}}_i + \int_0^{2\pi} \int_0^{\pi} \hat{\mathbf{r}}_s p_i(\theta, \phi) \sin\theta d\theta d\phi \right]. \tag{47}$$

Consequently,

$$\int_0^{2\pi} \int_0^{\pi} \hat{\mathbf{r}}_s p_i(\theta, \phi) \sin\theta d\theta d\phi = \frac{1}{2} i z_0 k Q_i \hat{\mathbf{r}}_i. \tag{48}$$

This development shows that diffraction about the rigid sphere increases the dipole moment by 50%, moving the acoustic center farther from the surface. Equation (48) is thus a theoretical proof of Vanderkooy's qualitative assertion that the KHIE pressure term moves the acoustic center away from the origin.[22]

Treating a quasi-arbitrary, continuous surface velocity distribution $u_n(\theta, \phi)$ as a distribution of point sources allows further generalization of Eq. (43) to

$$\mathbf{r}_c = \frac{3}{2} a \left[\frac{\int_0^{2\pi} \int_0^{\pi} u_n(\theta, \phi)\hat{\mathbf{r}}_s \sin\theta d\theta d\phi}{\int_0^{2\pi} \int_0^{\pi} u_n(\theta, \phi) \sin\theta d\theta d\phi} \right]$$

$$= \frac{3}{2} \left[\frac{\int_0^{2\pi} \int_0^{\pi} u_n(\theta, \phi)\mathbf{r}_s \sin\theta d\theta d\phi}{\int_0^{2\pi} \int_0^{\pi} u_n(\theta, \phi) \sin\theta d\theta d\phi} \right]. \tag{49}$$

This key result provides an upper bound to the acoustic center's radial distance given that $u_n(\theta, \phi)$ has the same phase.

The maximum distance $r_c = 3a/2$ occurs when all volume velocity concentrates at a single point.

V. GENERALIZATION TO NONSPHERICAL SOURCE CONFIGURATIONS

While the surface velocity and pressure in the KHIE provided the bases for the preceding spherical-source acoustic centering developments, one may generalize the approach using a notional observation sphere of minimal radius a that entirely envelops an acoustic source of arbitrary shape. Because of the uniqueness of the exterior solution in spherical coordinates, the pressure *or* particle velocity on the sphere will infer the monopole and dipole moments (for $ka \ll 1$) directly from its expansion coefficients.[27,29] If a monopole and dipole field uniquely determine the pressure produced by the source, the pressure or particle velocity on the sphere will provide the unique solution for $r \geq a$.[27] Consequently, a multipole expansion applied to the observed quantity must converge to the same monopole and dipole moments of the isolated source. Researchers have applied similar concepts in other works;[42,52,53] however, the nonuniqueness of the field inside the sphere requires additional consideration.[54]

Because multipole expansions and pressure-field expansions involving spherical harmonics and spherical Bessel functions have similar terms,[27–29] an equating of terms allows one to establish the relationships between the multipole moments and the pressure expansion coefficients. This approach is valid for constructing the exterior field, as Secs. V A and V B demonstrate, but the calculated monopole and dipole moments only have the physical meanings defined by Eqs. (4) and (5) in the limit of $ka \ll 1$. The surface integrals and spherical harmonic expansion coefficients do not have guaranteed relationships for higher frequencies, but this fact presents little problem for the following developments because the formulation of Eq. (10) is already in the limit of $ka \ll 1$.

A. General formulation

The Helmholtz equation solution in spherical coordinates is[27]

$$p(r, \theta, \phi, k) = \sum_{n=0}^{\infty} \sum_{m=-n}^{n} C_n^m h_n^{(2)}(kr) Y_n^m(\theta, \phi), \quad r \geq a, \tag{50}$$

where

$$C_n^m = \frac{1}{h_n^{(2)}(ka)} \int_0^{2\pi} \int_0^{\pi} p(a, \theta, \phi)\left[Y_n^m(\theta, \phi)\right]^* \sin\theta d\theta d\phi. \tag{51}$$

In practice, the expansion coefficients follow from discrete measurements of the pressure field around the source and numerical integration or a least squares fit.[55,56] Significantly, because the present work's formulation requires only expansion degrees up to $n = 1$, the low-frequency acoustic center could follow from only four sampled positions.[55]

Comparing Eqs. (50) and (19) reveals that

$$U_n^m = -\frac{1}{iz_0} C_n^m h_n^{(2)\prime}(ka).$$ (52)

Substitution of this result into Eqs. (14) and (11) yields the monopole moment

$$M = -ka^2 h_0^{(2)\prime}(ka)\sqrt{4\pi} C_0^0.$$ (53)

However, since $ka \ll 1$,

$$h_0^{(2)\prime}(ka) \approx -\frac{i}{(ka)^2}$$ (54)

and the monopole term simplifies to

$$M \approx i\frac{\sqrt{4\pi}}{k} C_0^0$$ (55)

(compare Ref. 27, p. 198).

For the dipole moment,

$$\mathbf{D}(\mathbf{0}) = -\frac{3}{2} ka^3 h_1^{(2)\prime}(ka)\sqrt{\frac{2\pi}{3}} \begin{bmatrix} C_1^{-1} - C_1^1 \\ -i(C_1^{-1} + C_1^1) \\ \sqrt{2}C_1^0 \end{bmatrix}.$$ (56)

Using the $ka \ll 1$ approximation

$$h_1^{(2)\prime}(ka) \approx -\frac{2i}{(ka)^3},$$ (57)

the dipole term simplifies to

$$\mathbf{D}(\mathbf{0}) = \frac{i\sqrt{6\pi}}{k^2} \begin{bmatrix} C_1^{-1} - C_1^1 \\ -i(C_1^{-1} + C_1^1) \\ \sqrt{2}C_1^0 \end{bmatrix}.$$ (58)

The acoustic center then follows from Eq. (10) as

$$\mathbf{r}_c = \frac{1}{kC_0^0}\sqrt{\frac{3}{2}} \begin{bmatrix} C_1^{-1} - C_1^1 \\ -i(C_1^{-1} + C_1^1) \\ \sqrt{2}C_1^0 \end{bmatrix},$$ (59)

but it is now in terms of the pressure-field expansion coefficients.

B. Point source distribution

An arbitrary point source distribution with quasi-arbitrary, real-number–related source strengths provides a simple nonspherical evaluation case because one can infer the exact value of r_c from the standard monopole and dipole moment definitions for point sources in free space.[22,30] For N point sources, the monopole moment is

$$M = iz_0 k \sum_{i=1}^{N} Q_i,$$ (60)

the dipole moment is

$$\mathbf{D}(\mathbf{0}) = iz_0 k \sum_{i=1}^{N} Q_i \mathbf{r}_i,$$ (61)

and the acoustic center is

$$r_c = \left(\frac{\sum_{i=1}^{N} Q_i \mathbf{r}_i}{\sum_{i=1}^{N} Q_i} \right).$$ (62)

This center-of-mass–like formula[57] is similar to Eqs. (43) and (49) but without the $3a/2$ scaling factor. Previously, the factor arose from the dipole moment formed from the diffraction around the spherical rigid body, as shown by Eq. (48) (also compare Ref. 58). However, center-of-mass–like formulas for nonspherical rigid boundaries and their velocity distributions will likely differ. Also, similar to Eq. (43), a real-vaued acoustic center follows when the relative source strength ratios of all point sources are real valued.

Suppose a spherical array of radius $R = 1.0$ m and $5°$ equiangular spacing in the polar and azimuthal angles samples the pressure field produced by five point sources with the amplitudes and positions listed in Table II at $kR = 0.01$. The spherical harmonic expansion coefficients follow from Chebyshev numerical integration,[56] such that Eq. (59) yields the acoustic center $\mathbf{r}_c = (0.92, -1.58, -0.20)$ m. This calculated value from the expansion coefficients agrees with that produced by Eq. (62) to less than a thousandth of a percent. As $kR \to 0$, the error decreases to machine precision.

Figure 9 depicts the resultant field produced by the point sources. The solid black circle denotes the sampling sphere in which all contours are missing to allow better visualization for $r < R$. The specific source amplitudes and positions create a strong dipole moment, causing the acoustic center to fall outside the sampling sphere. However, its location does not impact the validity of the spherical harmonic expansion in Eq. (50). The only requirement is that all non-homogeneous terms, i.e., the point sources, fall within the sphere so that the region $r \geq R$ satisfies the homogeneous Helmholtz equation.

VI. EXPERIMENTAL EXAMPLE

The results of a pertinent acoustic centering experiment and comparisons with the results of other centering methods provide further validation of the preceding developments. The authors employed a rotating semicircular microphone array to sweep out a sphere of sampled pressure data and evaluate the directivities of a KEMAR HATS with and without an attached torso and with varying head orientations.[59] The measurement and signal-processing techniques were similar to those used earlier for live speech.[36] The processing employed complex-valued frequency response functions (FRFs) and numerical integration[56] to produce the pressure expansion coefficients C_n^m described in Eq. (51). An $N = 10$

Samuel D. Bellows and Timothy W. Leishman   3413

TABLE II. Tabulated amplitudes and locations for five point sources inside a measurement sphere of radius $R = 1$ m.

Q_i (m^3/s)	x (m)	y (m)	z (m)
1.0	0.3	−0.1	−0.2
−0.6	0.3	0.3	0
0.7	0.2	−0.3	0
−0.8	−0.3	0.3	−0.1
0.2	−0.2	−0.3	0.1

expansion ensured that the area-weighted directivity factor function deviation (AWDFFD) level L_Q between the measured and expanded pressure[59] remained less than 0.1 dB for the frequencies of interest.[56]

As shown in Fig. 10, this HATS experiment extended the earlier work to consider the effects of attached manikin legs and a chair. The minimum sphere encompassing the entire arrangement had a radius $a \approx 0.75$ m with a center offset from the array's geometric center. However, if one considers the low-frequency scattering of selected manikin and chair parts to be neglible, a could become considerably smaller. To accommodate the configuration, the microphone radius increased from $R = 0.97$ m, used in Ref. 59, to $R = 1.17$ m. However, the enlarged radius still prohibited the exact alignment of the HATS mouth, the geometric center of the manikin's radiating region, at the array's geometric center. Consequently, post-processed acoustic centering became particularly important for correcting the measured directivity patterns (see Sec. VI B).

A. Centering results

In addition to calculating the source low-frequency acoustic center via Eq. (59), the authors considered four previously proposed acoustic centering algorithms to predict the acoustic center at various frequencies. The latter work involved minimizing the objective functions J_{ss} [Eq. (7.1) of Ref. 9], based on the coherent summation of the complex pressure; J_{lo} [Eq. (7.3) of Ref. 9 and Eq. (34) of Ref. 11], which penalizes energy in higher degree expansion terms;

FIG. 9. (Color online) Pressure produced by a point source distribution and the associated acoustic center marked as a green dot.

FIG. 10. (Color online) KEMAR HATS seated within a directivity measurement system.

J_{zo} [Eq. (30) of Ref. 11], which favors energy in the C_0^0 coefficient; and J_{ph} [Eq. (58) of Ref. 12], which considers phase symmetries. Technically, one should evaluate J_{ph} for phase symmetries in three orthogonal planes; however, radiation symmetry allowed optimization over the median (x-z) plane to suffice for the present example.

Figure 11 plots the objective functions in the median plane at 100 Hz ($ka \lesssim 1.4$). The manikin faces the positive x-direction and the array origin falls roughly at the manikin's chest. The solid black circle represents the measurement sphere circumference, whereas the surface colors and contours indicate the relative levels of the objective functions. Normalization between 0 and 1 for all objective functions facilitates simpler comparisons. The red $\times$ at $\mathbf{r}_c = (x, z) = (0.00, 0.27)$ m indicates the low-frequency acoustic center in this plane calculated from Eq. (59). As mentioned in Sec. II, this equation may sometimes produce a complex-valued acoustic center (also see Sec. VII). At this frequency, the imaginary part from the measured data were smaller by more than an order of magnitude than the real part and was consequently considered negligible. The calculated acoustic center aligns well with all objective function minima, producing excellent agreement with the outcomes of the previous works. The root-mean-square (RMS) deviations between the global objective function minima and low-frequency acoustic center were all less than 1 cm even though the localized acoustic center from Eq. (59) resulted from a simple closed-form solution rather than a computationally expensive optimization routine.

Figure 12 plots the four objective functions at 300 Hz ($ka \lesssim 4.1$) and the calculated low-frequency center appearing at $\mathbf{r}_c = (0.00, 0.25)$ m. Although this frequency exaggerates the low-frequency assumption, it is still instructive to consider the robustness of the calculated acoustic center. Because the radiation is slightly more directional at this frequency, local minima appear in some of the objective functions, although their global minima remain clear. The low-frequency acoustic center generally aligns well with the
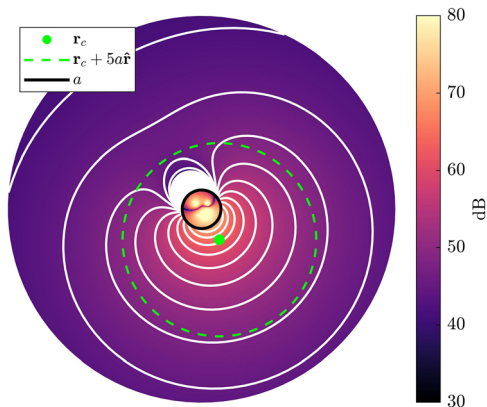
FIG. 11. (Color online) Objective functions in the median plane at 100 Hz: (a) J_{ss}, (b) J_{zo}, (c) J_{lo}, and (d) J_{ph}. The red × is the low-frequency acoustic center from Eq. (59).

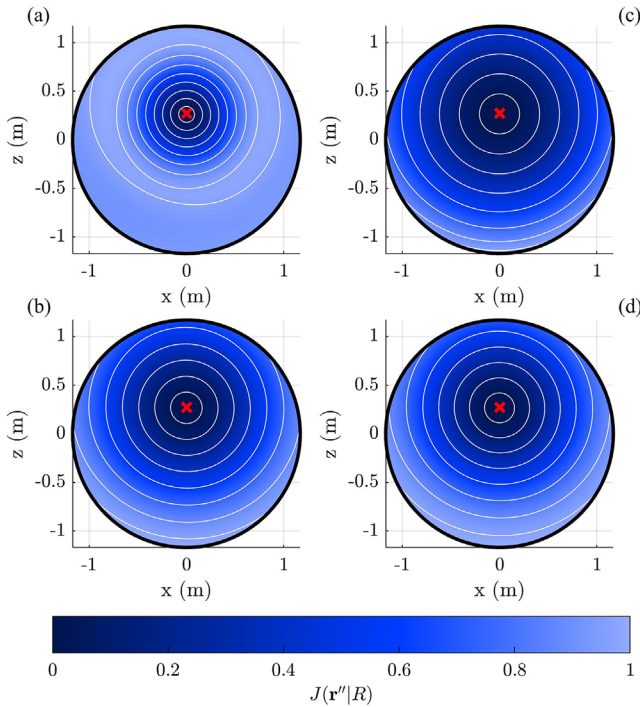FIG. 12. (Color online) Objective functions in the median plane at 300 Hz: (a) J_{ss}, (b) J_{zo}, (c) J_{lo}, and (d) J_{ph}. The red × is the low-frequency acoustic center from Eq. (59).

global minima but the agreement is not as exact at this frequency. Additionally, while the imaginary part of the calculated acoustic center is still relatively small, it has risen to within an order of magnitude of the real part, which further suggests that the low-frequency approximation has begun to break down. The RMS deviations between the global minima of the objective functions and the calculated acoustic center are less than 2 cm for J_{ss} and J_{zo} and 1 cm for J_{lo} and J_{ph}. For higher frequencies, the low-frequency acoustic center could serve as a viable initialization position to help the centering optimization routines achieve faster convergences.

B. Directivity correction

Figure 13 presents the normalized directivity balloons for the seated HATS at 100 and 300 Hz and illustrates the effectiveness of acoustic centering to correct near-field directivity pattern anomalies. The balloons employ colors and radii to depict relative levels on a 40 dB scale. The vantage point is from the right-hand side of the manikin, which faces the 0° azimuthal marker.

Figure 13(a) shows the measured 100 Hz directivity pattern at the array surface, expanded via spherical harmonics to degree $N = 10$. Although one would anticipate omnidirectional radiation at this frequency,[36] the source placement within the array causes the directivity to appear directional. As discussed by the authors in Ref. 60, far-field projection of the measured results allows the correction of such near-field anomalies. Figure 13(b) shows the 100 Hz far-field directivity balloon, projected via the $N = 10$ degree
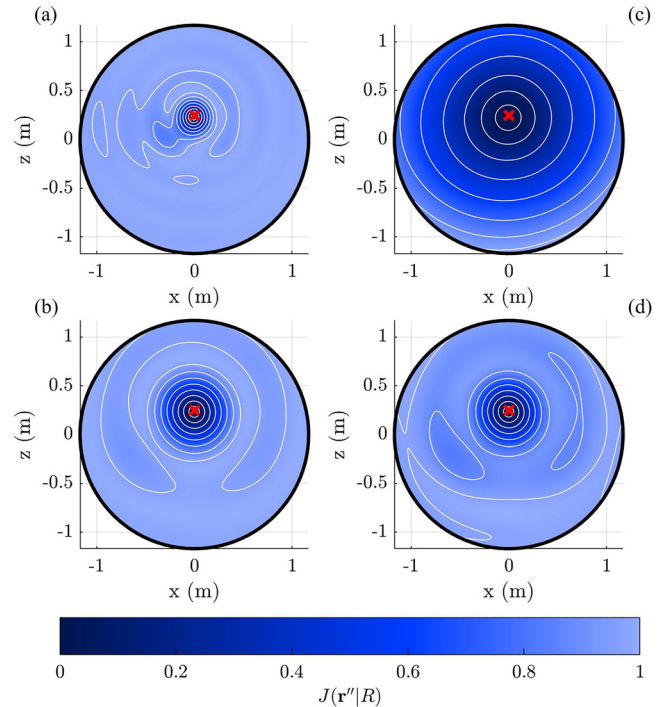
expansion. The far-field directivity is essentially omnidirectional, although the levels below the talker are minimally reduced, perhaps due to diffraction about the manikin's body and chair. Figure 13(c) plots the directivity evaluated at $r = 1.5$ m ($kr \approx 2.7$ and $r/2a \gtrsim 1.0$) but recentered about the low-frequency acoustic center presented in Fig. 11. Despite not being at a far-field evaluation distance, the directivity pattern appears nearly identical to the projected far-field pattern. The AWDFFD L_Q[59] is only 0.1 dB between the far-field and $r = 1.5$ m centered patterns but 1.6 dB between the far-field and $r = R = 1.17$ m measured patterns.

Figure 13(d) shows the measured 300 Hz directivity pattern at the array surface, again expanded to degree $N = 10$. At this higher frequency, diffraction led to reduced levels behind and below the manikin and chair.[36,48] The axis of maximum radiation appears upward in elevation from the mouth axis, which is not characteristic for this particular frequency.[36] Figure 13(e) shows the projected far-field directivity, determined using the $N = 10$ expansion, with the axis of maximum radiation falling directly in front of the manikin's mouth. Finally, Fig. 13(f) shows the centered directivity pattern evaluated at $r = 1.5$ m ($kr \approx 8.2$ and $r/2a \gtrsim 1.0$). The centering improved L_Q from 1.4 to 0.7 dB relative to the projected far-field pattern.

VII. DISCUSSION

The low-frequency acoustic center provides a valuable and straightforward means to treat a distributed source as a single point source. However, its validity depends upon the

J. Acoust. Soc. Am. **153** (6), June 2023

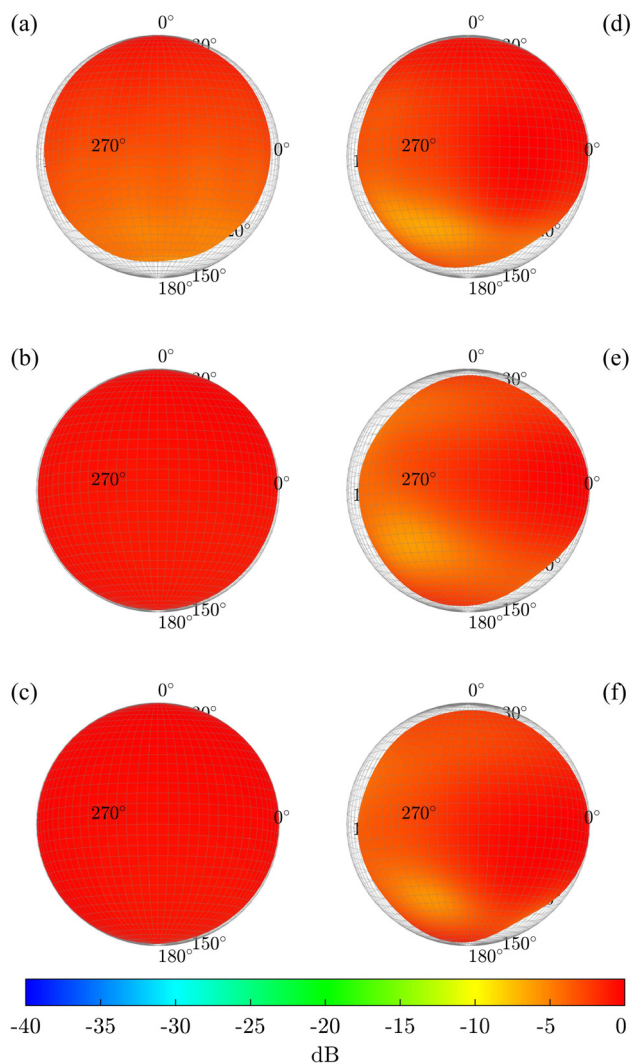Samuel D. Bellows and Timothy W. Leishman   3415

FIG. 13. (Color online) KEMAR HATS directivity. (a) $r = R = 1.17$ m measured, (b) far-field projected, and (c) $r = 1.5$ m centered at 100 Hz. (d) $r = R = 1.17$ m measured, (e) far-field projected, and (f) $r = 1.5$ m centered at 300 Hz.

nature of the source and the observation distance. For example, a radially oscillating sphere whose acoustic center falls at the origin has an equivalent point source representation valid in the near and far fields. On the other hand, two point sources at opposing poles on a sphere with a strength ratio $\gamma = -0.8$ (see Sec. IV E) have an equivalent point source representation that is not valid until the observation distance is many times the sphere's radius. Thus, while the low-frequency acoustic center is generally valid at a sufficient distance for sources producing omnidirectional far-field directivities, it is judicious to consider the minimum distance at which the equivalent representation becomes acceptable for practical applications.

The low-frequency centering method discussed in this work permits the direct use of spherical harmonic expansion coefficients from the acoustic pressure or particle velocity over an observation sphere. This resource is advantageous because it supports the direct determination of an acoustic center without requiring computationally expensive centering algorithms. Although it is not valid at higher frequencies, the low-frequency acoustic center may be a good starting point to improve the performance of higher-frequency, spherical harmonic-based optimization techniques. While this work employed spherical harmonic expansions to determine the dipole and monopole moments, these moments could instead follow from numerically integrating Eqs. (4) and (9). As boundary element methods (BEM) yield the surface pressure and normal particle velocity for a given source configuration, computing the low-frequency acoustic center would be a simple post-processing step in numerical simulations. Additionally, numerically evaluated higher-order multipole moments could serve as a basis for generalizing this work to higher frequencies.

While the results of this work support the efficacy of defining the acoustic center in terms of the location of an equivalent point source, this definition can become problematic in some situations. Replacing an extended source with an equivalent point source requires first that $ka \ll 1$ and second that the far-field source radiation is omnidirectional.[22] These conditions highlight certain definitional weaknesses.

To begin with, because many sources produce complicated directional patterns at higher frequencies, replacing their *entire* respective pressure fields with a single equivalent point source is equivocal for broad bandwidths. Simple omnidirectional far-field radiation allowed good agreement between the distributed sources and their equivalent point source representations shown in Figs. 3, 4, and 6. However, complex directional patterns appearing at higher frequencies would require higher-order moments for an accurate representation.

Furthermore, even at low frequencies, some sources do not radiate omnidirectionally in the far field. For example, Weinreich's "sound hole sum rule," developed during his violin directivity studies, showed that sources with sound holes or ports connecting an interior cavity to the exterior domain may develop intense dipole moments and vanishing monopole moments.[61] These and other directional low-frequency source configurations[30] further limit the centering approach. For Eq. (7) to remain valid, one must ostensibly define what type of radiation is sufficiently omnidirectional.

Instead of a global representation of the entire sound field at higher frequencies, one could attempt to match the pressure field only in a specified direction and position, as in Trott's redefinition.[16] This approach may be beneficial for some practical broadband applications, such as transducer calibrations.[4,5,17,19] Nonetheless, Jacobsen *et al.*[17] showed that this concept leads to an acoustic center that varies with the observation position **r**. Only in the far field do some of these centering approaches converge to the unique solution of Eq. (10), as seen in Fig. 2. Variations in the acoustic center dependent on observation position limit the application of the approach to centering directivity patterns, which require a unique acoustic center. Additionally, the different methods based on this concept do not give a consistent location at higher frequencies, even at a far-field observation

Samuel D. Bellows and Timothy W. Leishman

distance. More recent centerings of higher-frequency musical instrument directivities have likewise given inconsistent results for the same sources when employing different objective functions.[9,11,12]

Finally, the center-of-mass–like formulas of Secs. IV F and V B reveal that some source distributions with complex-valued source strengths or surface velocities may lead to complex-valued acoustic centers with ambiguous meanings. A simple example of such a configuration is a loudspeaker with two drivers driven 90° out of phase. Accordingly, the low-frequency acoustic centering developments of this work require careful implementation. Using quasi-arbitrary, real-number–related source strengths and surface velocities kept the acoustic centers real. The experimental results in Sec. VI A yielded acoustic centers that were also nearly real. However, based on Eq. (10), some sources may have undefined low-frequency acoustic centers or centers that are considerably distant from the source body.

Hence, defining the acoustic center as the position of an equivalent point source perhaps best applies as a limiting case for low-frequency radiation from primarily far-field omnidirectional sources. The need remains for a more consistent definition of the acoustic center, applying to all sources and generalizing to all frequencies. In principle, it should reduce to Trott's redefinition[16] and the acoustic center discussed in this work for low frequencies and far-field omnidirectional sources.

VIII. CONCLUSIONS

This work has revisited the concept of a low-frequency acoustic source center and set forth a straightforward centering formula based on monopole and dipole moments. Application to the sphere produced a simple closed-form solution for the acoustic center of a quasi-generally vibrating spherical source. Spherical harmonic expansions of pressure fields from quasi-arbitrary source distributions also allow the determination of their acoustic centers, and center-of-mass–like formulas yield insights into the center locations for many source configurations.

The concept of an acoustic center corresponding to a single point source limits the method for some distributed sources because it precludes application to higher frequencies or sources with vanishing monopole moments. Future research could address this problem and clarify the meaning of the acoustic center for all sources and frequencies. It could also apply centering techniques to other theoretical or measured sources to produce additional insights. The authors encourage further work in these areas.

ACKNOWLEDGMENTS

[1]ANSI Standard S1.1-2004: *American National Standard Acoustical Terminology* (Acoustical Society of America, New York, 2004).

[2]IEC 61094-3-2016, "Electroacoustics-measurement microphones-Part 3: Primary method for free-field calibration of laboratory standard microphones by the reciprocity technique" (International Electrotechnical Commission, Geneva, Switzerland, 2016).

[3]M. Vorländer and H. Bietz, "Novel broad-band reciprocity technique for simultaneous free-field and diffuse-field microphone calibration," Acta Acust. Acust. **80**, 365–367 (1994).

[4]R. P. Wagner and V. Nedzelnitsky, "Determination of acoustic center correction values for type LS2aP microphones at normal incidence," J. Acoust. Soc. Am. **104**(1), 192–203 (1998).

[5]S. Barrera-Figueroa, K. Rasmussen, and F. Jacobsen, "The acoustic center of laboratory standard microphones," J. Acoust. Soc. Am. **120**(5), 2668–2675 (2006).

[6]G. R. Hruska and W. Koidan, "Free-field method for sound-attenuation measurement," J. Acoust. Soc. Am. **58**(2), 507–509 (1975).

[7]K. A. Cunefare, V. B. Biesel, J. Tran, R. Rye, A. Graf, M. Holdhusen, and A.-M. Albanese, "Anechoic chamber qualification: Traverse method, inverse square law analysis method, and nature of test signal," J. Acoust. Soc. Am. **113**(2), 881–892 (2003).

[8]ISO 3745:2012, "Acoustics - Determination of sound power levels and sound energy levels of noise sources using sound pressure - Precision methods for anechoic rooms and hemianechoic rooms" (International Organization for Standardization, Geneva, Switzerland, 2012).

[9]D. Deboy, "Acoustic centering and rotational tracking in surrounding spherical microphone arrays," Master's thesis, Institute of Electronic Music and Acoustics, University of Music and Performing Arts, Graz, Austria, 2010.

[10]D. Deboy and F. Zotter, "Tangential intensity algorithm for acoustic centering," in *Proceedings of the 37th German Annual Conference on Acoustics (DAGA 2011)*, Düsseldorf, Germany (2011), pp. 321–322.

[11]I. Ben Hagai, M. Pollow, M. Vorländer, and B. Rafaely, "Acoustic centering of sources measured by surrounding spherical microphone arrays," J. Acoust. Soc. Am. **130**(4), 2003–2015 (2011).

[12]N. R. Shabtai and M. Vorländer, "Acoustic centering of sources with higher-order radiation patterns," J. Acoust. Soc. Am. **137**(4), 1947–1961 (2015).

[13]M. S. Ureda, "Apparent apex theory," in *Audio Engineering Society Convention* (1978), p. 61.

[14]M. S. Ureda, "Apparent apex revisited," in *Audio Engineering Society Convention* (1991), p. 90.

[15]M. S. Ureda, "Apparent apex, part III: The three-dimensional case," in *Audio Engineering Society Convention* (1991), p. 91.

[16]W. J. Trott, "Effective acoustic center redefined," J. Acoust. Soc. Am. **62**(2), 468–469 (1977).

[17]F. Jacobsen, S. B. Figueroa, and K. Rassmussen, "A note on the concept of acoustic center," J. Acoust. Soc. Am. **115**(4), 1468–1473 (2004).

[18]J. R. Cox, "Physical limitations on free-field microphone calibration, Ph.D. thesis, Massachusetts Institute of Technology, Cambridge, MA, 1954.

[19]K. Rasmussen, "Acoustic centre of condenser microphones," The Acoustics Laboratory, Technical University of Denmark, Report No. 5 (1973).

[20]ANSI S1.10-1966: *Method for Calibration of Microphones* (Acoustical Society of America, New York, 1966).

[21]S. Morita, N. Kyono, S. Sakai, T. Yamabuchi, and Y. Kagawa, "Acoustic radiation of a horn loudspeaker by the finite element method–a consideration of the acoustic characteristic of horns," J. Audio Eng. Soc. **28**(7/8), 482–489 (1980).

[22]J. Vanderkooy, "The acoustic center: A new concept for loudspeakers at low frequencies," Audio Eng. Soc. Conv. **121**, 1–15 (2006).

[23]J. Vanderkooy and D. Henwood, "Polar plots for low frequencies: The acoustic centre," Audio Eng. Soc. Conv. **120**, 1–10 (2006).

[24]J. Vanderkooy, "Applications of the acoustic centre," Audio Eng. Soc. Conv. **122**, 1–11 (2007).

[25]J. Vanderkooy, "The low-frequency acoustic center: Measurement, theory, and application," Audio Eng. Soc. Conv. **128**, 1–24 (2010).

[26]R. M. Aarts and A. J. E. M. Janssen, "Comparing sound radiation from a loudspeaker with that from a flexible spherical cap on a rigid sphere," J. Audio Eng. Soc. **59**(4), 201–212 (2011).

[27]E. G. Williams, *Fourier Acoustics: Sound Radiation and Nearfield Acoustical Holography* (Academic Press, London, 1999).

[28]P. M. Morse and K. U. Ingard, *Theoretical Acoustics* (Princeton University Press, Princeton, NJ, 1968).

[29]T. Martin and A. Roure, "Optimization of an active noise control system using spherical harmonics expansion of the primary field," J. Sound Vib. **201**(5), 577–593 (1997).

[30]A. D. Pierce, *Acoustics* (Springer International Publishing, Cham, Switzerland, 2019).

[31]L. Beranek and T. Mellow, *Acoustics: Sound Fields, Transducers and Vibration*, 2nd ed. (Academic Press, Cambridge, MA, 2019).

[32]T. F. Johansen, "On the directivity of horn loudspeakers," J. Audio Eng. Soc. **42**(12), 1008–1019 (1994) available at http://www.aes.org/e-lib/browse.cfm?elib=6913.

[33]M. A. Gerzon, "Maximum directivity factor of *n*th-order transducers," J. Acoust. Soc. Am. **60**(1), 278–280 (1976).

[34]H. Dunn and D. W. Farnsworth, "Exploration of pressure field around the human head during speech," J. Acoust. Soc. Am. **10**, 184–199 (1939).

[35]A. H. Meyer and J. Meyer, "The directivity and auditory impressions of singers," Acustica **58**, 130–140 (1985).

[36]T. W. Leishman, S. D. Bellows, C. M. Pincock, and J. K. Whiting, "High-resolution spherical directivity of live speech from a multiple-capture transfer function method," J. Acoust. Soc. Am. **149**(3), 1507–1523 (2021).

[37]D. W. Martin, "Directivity and the acoustic spectra of brass wind instruments," J. Acoust. Soc. Am. **13**(3), 309–313 (1942).

[38]H. F. Olson, *Musical Engineering: An Engineering Treatment of the Interrelated Subjects of Music, Musical Instruments, Speech, Acoustics, Sound Reproduction and Hearing* (McGraw-Hill, New York, 1952).

[39]J. Meyer, *Acoustics and the Performance of Music: Manual for Acousticians, Audio Engineers, Musicians, Architects, and Musical Instrument Makers*, 5th ed, Modern Acoustics and Signal Processing (Springer Science & Business Media, New York, 2009).

[40]K. J. Bodon, "Development, evaluation, and validation of a high-resolution directivity measurement system for played musical instruments," Master's thesis, Brigham Young University, Provo, UT, 2016.

[41]J. Weinberger, H. F. Olson, and F. Massa, "A uni-directional ribbon microphone," J. Acoust. Soc. Am. **5**(2), 139–147 (1933).

[42]W. Williams, N. G. Parke, D. A. Moran, and C. H. Sherman, "Acoustic radiation from a finite cylinder," J. Acoust. Soc. Am. **36**(12), 2316–2322 (1964).

[43]E. A. G. Shaw, "Transformation of sound pressure level from the free field to the eardrum in the horizontal plane," J. Acoust. Soc. Am. **56**(6), 1848–1861 (1974).

[44]H. Møller, M. F. Sørensen, D. Hammershøi, and C. B. Jensen, "Head-related transfer functions of human subjects," J. Audio Eng. Soc. **43**(5), 300–321 (1995).

[45]V. P. Sivonen and W. Ellermeier, "Directional loudness in an anechoic sound field, head-related transfer functions, and binaural summation," J. Acoust. Soc. Am. **119**(5), 2965–2980 (2006).

[46]T. M. Dunster, *NIST Handbook of Mathematical Functions* (Cambridge University Press, New York, 2010).

[47]E. Skudrzyk, *The Foundations of Acoustics: Basic Mathematics and Basic Acoustics* (Springer-Verlag, New York, 1971).

[48]S. D. Bellows and T. W. Leishman, "Modeling musician diffraction and absorption for artificially excited clarinet directivity measurements," Proc. Mtgs. Acoust. **46**(1), 035002 (2022).

[49]M. Otani, H. Shigetani, M. Mitsuishi, and R. Matsuda, "Binaural ambisonics: Its optimization and applications for auralization," Acoust. Sci. Technol. **41**, 142–150 (2020).

[50]J. L. Flanagan, "Analog measurements of sound radiation from the mouth," J. Acoust. Soc. Am. **32**(12), 1613–1620 (1960).

[51]T. Hélie and X. Rodet, "Radiation of a pulsating portion of a sphere: Application to horn radiation," Acta Acust. united Acust. **89**(4), 565–577 (2003).

[52]N. H. L. Bouchet, T. Loyau, and C. Boisson, "Calculation of acoustic radiation using equivalent-sphere methods," J. Acoust. Soc. Am. **107**, 2387–2397 (2000).

[53]S. F. Wu, *The Helmholtz Equation Least Squares Method: For Reconstructing and Predicting Acoustic Radiation* (Springer, New York, 2015).

[54]T. Rother and S. C. Hawkins, "Notes on Rayleigh's hypothesis and the extended boundary condition method," J. Acoust. Soc. Am. **149**(4), 2179–2188 (2021).

[55]B. Rafaely, *Fundamentals of Spherical Array Processing* (Springer-Verlag, Berlin Heidelberg, 2015), Vol. 8.

[56]S. D. Bellows and T. W. Leishman, "Spherical harmonic expansions of high-resolution musical instrument directivities," Proc. Mtgs. Acoust. **35**, 035005 (2018).

[57]R. D. Gregory, *Classical Mechanics* (Cambridge University Press, Cambridge, UK, 2006).

[58]G. W. Elko, "An acoustic vector-field probe with calculable obstacle bias," in *NOISE-CON 91 Proceedings* (1991), pp. 525–527.

[59]S. Bellows and T. W. Leishman, "Effect of head orientation on speech directivity," in *Proceedings of Interspeech 2022* (2022), pp. 246–250.

[60]S. D. Bellows and T. W. Leishman, "Acoustic source centering of musical instrument directivities using acoustical holography," Proc. Mtgs. Acoust. **42**(1), 055002 (2020).

[61]G. Weinreich, "Sound hole sum rule and the dipole moment of the violin," J. Acoust. Soc. Am. **77**(2), 710–718 (1985).